

A New Approach to Printer Calibration Based on Nested Gamut Shells

Patrick G. Herzog
Aachen University of Technology, Technical Electronics Institute
Aachen, Germany

Abstract

A new method of printer calibration is based on the subdivision of the printer gamut into nested gamut shells. This is a further development of an analytical gamut surface representation published earlier.[1,2] For every gamut (sub)shell, an analytical relationship to the corresponding shell of the CMY cube is established from a measured set of test colors. Simple linear interpolation between the nested shells yields appropriate results for the whole volume. The transformation accuracy for practical printers is approx. 2.2 CIELAB units (mean error) and 8 units (maximum error) and is comparable with other calibration methods.

1. Introduction

A well-known problem of color reproduction is the general difficulty to predict the produced colors when a printer is controlled by certain color control signals (CMY(K) or RGB). There are two basic approaches to solve the problem. In the numerical approach, a representative (but comparatively small) subset of test colors is printed and then measured colorimetrically. Hence, a correspondence table between the control signals and the produced colors is achieved. This table has to be completed for all existing colors (usually $2^8 \times 2^8 \times 2^8 \approx 16 \cdot 10^6$) and inverted by special three-dimensional interpolation techniques. In practice, however, the table size is often reduced from 48 Mbytes (for three bytes per color) to a considerably smaller size with the trade-off that the missing entries must be computed from neighbored entries by interpolation in real-time.

The second approach is based on a description of the physical circumstances of a print process like the light reflection in the paper and the dyes. The Neugebauer model is a famous example.[3] A disadvantage of the physical models is the need to have comprehensive knowledge of the physical background of the specific process. Moreover, the models are mostly limited to a certain print process. While in recent years some physical models of rather good performance have been developed, the effort to develop and to handle such a model is growing with the achieved accuracy.

An alternative is the employment of neural networks.[4,5] The performance is comparable with other numerical methods (based on a comparable number of test data) but is still limited by computing time. Moreover, such systems respond very sensitively to colors that were badly represented by the training set.

2. A New Method of Printer Calibration

The new approach described in this paper combines some advantages of the numerical and the physical models. Similar to numerical techniques, a limited set of test colors is printed and measured colorimetrically. Yet by the way of contrast, there is no need to build correspondence tables. Instead, a mostly analytical relationship between the control signals and the reproduced colors is established from the measured data set. The analytical relationship is a great advantage with respect to the amount of memory needed to represent the whole transformation. However, in contrast with physical models, there is no need to know any details of the printing process.

The principle of this method has already been successfully implemented for the analytical representation of gamut surfaces[1,2] and has been practically tested for gamut mapping.[6]

2.1. Basic Principles

The basic principles were already explained in refs. 1 and 2 but will be discussed here from a slightly different viewpoint. A typical color reproduction process is controlled by three color-control signals at the input. Let us consider a typical print process that is controlled by CMY colorant concentrations (CMY**K** processes can also be included in most cases if well-defined separation algorithms are used; see ref. 2). Controlled by the CMY signals, the printer produces colors that can be described by any of the well-known color spaces, e. g. CIELAB, CIEXYZ, or RLAB.[7,8]

In Fig. 1, the space of color-control signals CMY of a printer is presented. Each of the three control signals can be modified independently between 0% and 100%. There-

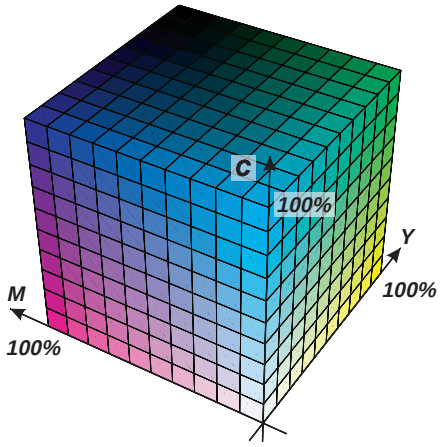

Figure 1: *The CMY cube of a printer.*

fore, all colors the device can produce are contained in a cube. This cube is called the *CMY cube* in the following discussion. The eight corners of the cube control the full- and zero-tone colors and all the integer mixtures of these colors.

All the colors the printer produces when being controlled by any of the triplets of color control signals make up the *color gamut* of the printer (Fig. 2). This color gamut is the result of the transformation of the CMY cube into the CIELAB space by the printer.

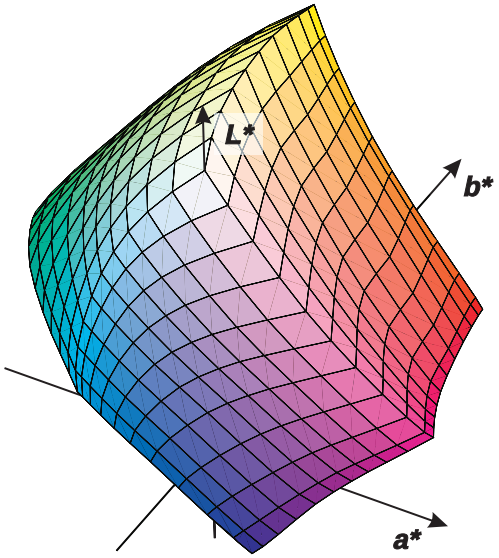

Figure 2: *The color gamut of a dye diffusion thermal printer.*

Since in practice, a given CIELAB color is to be reproduced by the printer and one has to know which control signals produce this exact color, the task of "calibrating the printer" can be translated into "inverting the transformation" initiated by the printer. The color gamut has some characteristics inherited from the CMY cube: it has eight corners, 12 edges and six planes. Hence it can be considered to be a *distorted cube*. From this point of view, "calibrating the printer" is equivalent with "removing the distortion introduced by the printer".

Therefore, we have to establish *inverse distortion functions* to transfer the color gamut back into a regular cube. For this purpose, two kinds of distortion functions and two scaling functions are used (we omit the term "inverse" since we treat only this one direction). All these functions together are referred to as *transformation functions* in the following.

2.2. Color Gamut and Kernel Gamut

The coordinates L*a*b* do not correspond to coordinates of the CMY space. However, this could be achieved by introducing new coordinates: one axis, combining both the black point and the white point of the CMY cube, corresponds with the lightness axis L*, and likewise two further axes orthogonal to the first (in CMY space) correspond with a* and b*, respectively.

In fact, we follow a more general approach by introducing a new mathematical space x, y, z (that has nothing in common with CIEXYZ) which is called the *kernel space*. Within this space, a unit cube is defined that is standing on its vertex and whose center is located at the origin of the kernel space (Fig. 3). This unit cube is called the *kernel gamut* in the following.

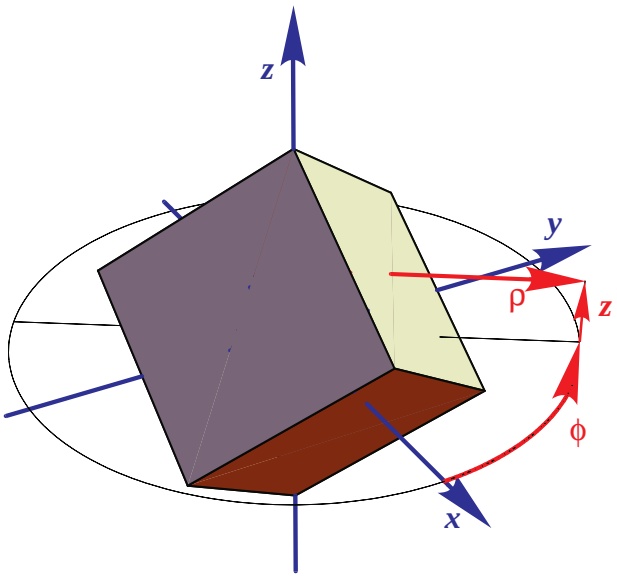

Figure 3: *The kernel gamut in the kernel space.*

The transformation is now subdivided into two steps where the color gamut is first mapped into the kernel gamut by the transformation functions. In the second step, the

kernel space can easily be transformed into the CMY space by a simple matrix operation. The following discussion will be mainly limited to the first step.

2.3. Nested Shells

Before the analytical transformation is established, the participating spaces (CIELAB and kernel space) are subdivided into nested shells within the limits of the respective gamuts. There are several potential ways of subdivision. One possibility is to organize the subshells concentrically, all including a fixed center point. This is disadvantageous for two reasons. First, the number of test colors rapidly decreases for inner-most shells. Second, a polar coordinate system that has its origin lying at the center point with one coordinate axis and two coordinate angles is needed to manage the data. This polar system is rather poorly correlating with colorimetric needs.

A much better choice is a cylindric coordinate system whose coordinates cylindric axis, radius, and angle perfectly fit to the colorimetric terms lightness, chroma, and hue. In this context, the nesting of the subshells is organized in a "cylindrical concentric" sense, i. e. each of the shells includes the gray axis within the range from black point to white point (Fig. 4). This structure ensures that the number of data points is not too small for inner shells. In fact, this kind of nesting has the disadvantage that the test chart to characterize the printer must be organized correspondingly.

The task of transforming between color space and kernel space is now reduced to the mapping of singular gamut shells from color gamut into kernel gamut. This is carried out by distortion of the gamut shell in order to form the corresponding regular shape of the kernel shell.

3. Transformations

3.1. Mapping of Gamut Shells

Before the analytical transformation can be defined, a suitable description of the gamut shells is required. The surface of a three-dimensional body can mathematically be expressed as a function of two variables. The simplest way is to choose the cylindric radius as a function of the cylindric axis and the angle. This applies both to the color space and the kernel space. In CIELAB we obtain C*(L*h*) and in kernel space $\rho(z, \phi)$, where C* = chroma, h* = hue; for z, ρ, ϕ cf. Fig. 3. Figures 5 and 6 show plots of the surfaces of the kernel gamut and the color gamut, respectively.

In ref. 2 a closed analytical expression is given to represent the function of Fig. 5. To map the color gamut's surface onto the kernel gamut's surface, two distortion and a scaling function are needed. The mapping is separated into

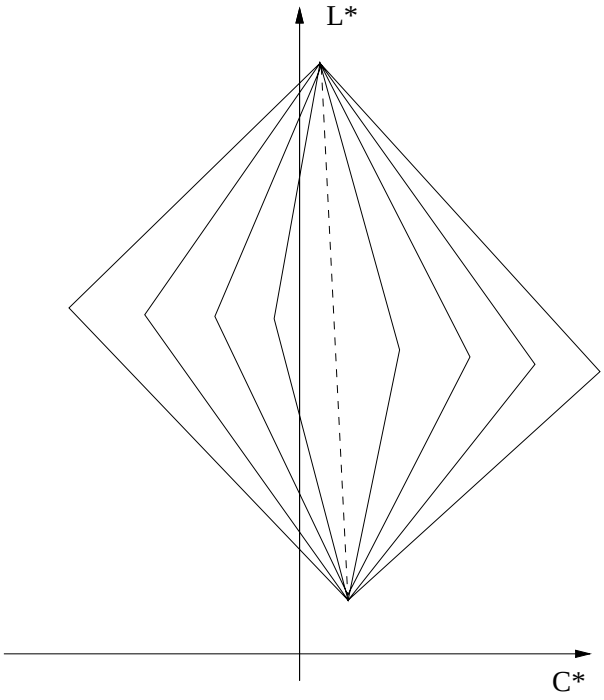

Figure 4: *The nesting of gamut shells.*

two consecutive steps. In a first step, two distortion functions $z_d(L^*, h^*)$ and $\phi_d(L^*, h^*)$ are introduced to move the edges, corners and planes of the color gamut to the correct positions in the kernel domain. In the second step, the amplitudes are adjusted by a scaling operation which is a combination of a multiplicative ($s(\phi)$) and an additive part ($s_a(z, \phi)$).

In Fig. 4 it can be seen that in general the black point and the white point are located off the grey axis. This is problematic since in regions near those points, no boundaries exist for a great part of the possible hue angles. The solution is to first transform the whole color gamut in such a way that the "device gray axis", i. e. the colors produced by C = M = Y, is mapped onto the L* axis. Since this operation is similar to tilting the color gamut, we call it "tilting".

To determine the tilting, the device gray axis is measured. Then, the trends of the a* and b* chrominances are interpolated over the lightness ($a_t(L^*)$ and $b_t(L^*)$) and subtracted from all colors:

$$L^{*\prime} = L^* \quad (1)$$

$$a^{*\prime} = a^* - a_t(L^*) \quad (2)$$

$$b^{*\prime} = b^* - b_t(L^*) \quad (3)$$

With this, the black and the white point of the color gamut as well as any other device-gray colors are mapped onto the L* axis. Hence, when later the color gamut is trans-

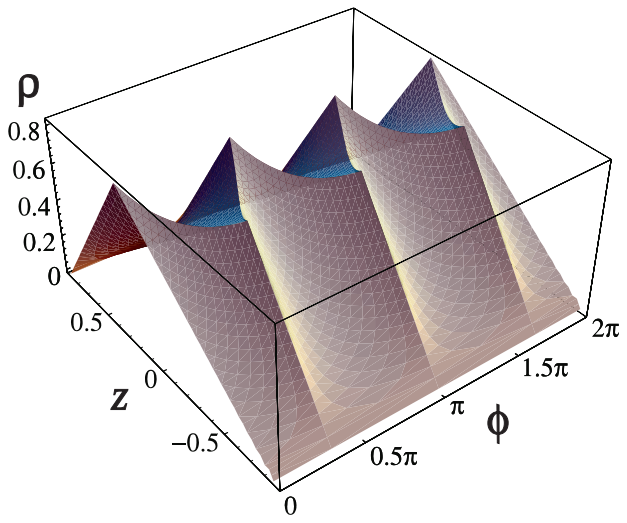

Figure 5: *The kernel gamut's surface in the 2D presentation.*

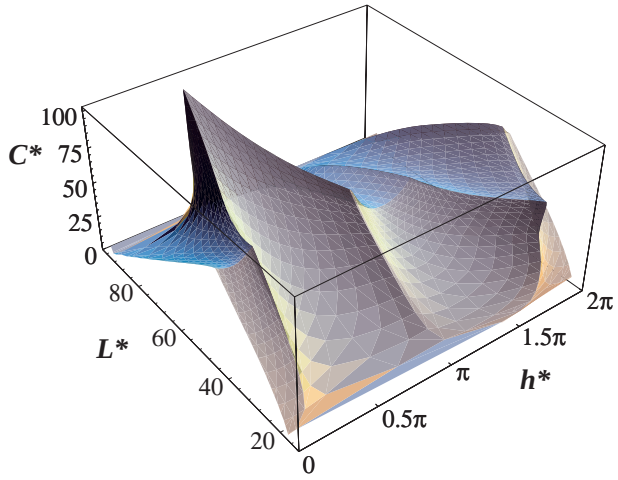

Figure 6: *The color gamut's surface in the 2D presentation.*

formed into the kernel gamut, the device-gray colors are mapped onto the z axis and then in the succeeding step onto the diagonal C = M = Y of the CMY space. Consequently, the grey colors are treated appropriately.

The transformation functions in principle are the same as given in ref. 2 except that some improvements have been made. The main difference is that the scaling is now defined completely in the (z, ϕ) domain instead of defining the additive scaling in the (L*h*) domain. This proved to yield better results for the transformation.

The transformation of a given color $L_0^* C_0^* h_0^*$ is carried out as follows.

1. Tilting according to eqs. (1)–(3).

2. Mapping into the kernel domain:

$$z_0 = z_d(L_0^{*\prime}, h_0^{*\prime}) \quad (4)$$

$$\phi_0 = \phi_d(L_0^{*\prime}, h_0^{*\prime}) \quad (5)$$

$$\rho_0 = \frac{C_0^{*\prime} - s_a(z_0, \phi_0)}{s(z_0, \phi_0)} \quad (6)$$

3. Transforming from kernel space into CMY space:

$$\begin{pmatrix} C_0 \\ M_0 \\ Y_0 \end{pmatrix} = \mathcal{R} \cdot \begin{pmatrix} \rho_0 \cos\phi_0 \\ \rho_0 \sin\phi_0 \\ z_0 \end{pmatrix} + \vec{\mathrm{t}}, \quad (7)$$

where $\vec{t}$ is a translation vector and $\mathcal{R}$ is a rotation and scaling matrix of the dimension 3×3. Since the kernel gamut as well as the CMY cube are identical objects for any arbitrary printing process, $\mathcal{R}$ and $\vec{t}$ remain the same for any arbitrary process and hence must be determined just once.

3.2. Mapping of Arbitrary Colors

In the above discussion, the transformation of colors contained in a well-known shell is described. In practical use, however, the transformation of arbitrary colors is required. For this purpose, a number of nested subshells are defined. In practice, the usage of the surface shell plus three subshells, giving a total of four nested shells, performed well. Additionally, the L* axis is treated as a "zero-shell", accompanied with the definition of an own function $z_d(L^*)$ but no own other functions.

Before a color can be transformed, its relative position in-between the shells is determined by comparison of its tilted chroma $C_0^{*\prime}$ with the chromas of the shells for the given pair of $L_0^{*\prime}, h_0^{*\prime}$. The closed analytical expression for the shells is derived from eqs. (4)–(6) and is given as follows:

$$\hat{C} = \hat{\rho}(z, \phi) \cdot s(z, \phi) + s_a(z, \phi) \quad (8)$$

$$\text{with} \quad z = z_d(L^{*\prime}, h^{*\prime}) \quad (9)$$

$$\text{and} \quad \phi = \phi_d(L^{*\prime}, h^{*\prime}) \quad (10)$$

$\hat{\rho}(z, \phi)$ is the closed analytical expression for the kernel gamut as given by ref. 2. Once the neighbored shells and their relative position to the given color are known, the values z_0, ϕ_0, and ρ_0 of the given color can be linearly interpolated from the respective values of the adjacent shells.

4. Performance

The optimization of the distortion and scaling functions is non-trivial because it is not linear. One can make use of software packages that allow non-linear curve-fitting of multidimensional functions with a high number of parameters. However, the proper choice of starting values for the parameters is a highly critical business. Here, algorithms have been developed that allow stable optimization of the

transformation functions for a large number of test devices (dye diffusion printers, ink jet, proof processes, printing machines). A description of these algorithms would be beyond the scope of this paper, it is reserved for a future paper.

The number of parameters to represent the transformation per shell is composed of 47 for z_d, 75 for ϕ_d, and 31 for the scaling. These 153 parameters are required for each of the four shells. One has to add five parameters for $z_d(L^*)$ of the zero-shell and 18 points (three coordinates each) for the representation of the grey axis. This leads to a total of 671 Parameters for the representation of the whole transformation.

The calibration was tested by generating two random sets of CIELAB colors (chromatic and achromatic) withing the limits of the color gamut. From these given colors, CMY values were computed that were used to control the printer. The produced colors were measured and converted into CIELAB coordinates. The differences between the given and the produced CIELAB colors were evaluated statistically (CIELAB and CIE94 ΔE). Currently, two print processes were employed: a thermal dye diffusion printer and the Neugebauer model of a proof process. The results are given by Table 1. One can recognize that

Table 1: *Transformation results (given as mean/max. values). Number of random colors: Neugebauer: 2000/200 (chromatic/achromatic); Thermal: 432/36 (chromatic/achromatic).*

	chromatic	achromatic
	ΔE_{ab} (mean/max.)	
Neugebauer	1.8 / 7.6	0.7 / 2.1
dye diffusion	2.5 / 8.0	2.2 / 5.6
	ΔE_{94} (mean/max.)	
Neugebauer	1.2 / 7.4	0.7 / 1.9
dye diffusion	1.9 / 6.6	2.0 / 4.6

the results for the model (Neugebauer) are better than for the real printer. This is due to the fact that characterizing a real print process contains a number of uncertainties like printer tolerances or measuring errors. It sometimes happens that two consecutive prints of the same test chart lead to differences of up to 1.4 CIELAB units between the measured data sets. These systematic errors occured to be mostly lightness shifts.

The number of measured test colors to characterize the print process was 626 in each case. For visual assessments, several images were printed using either the described, new calibration method or another method that was successfully used for many years and therefore was considered as a reference calibration method. When two images printed using different calibration methods were directly compared, some minor differences could be identified. However, none of the two methods was judged to be superior to the other. Hence, one can conclude that the new method of printer calibration can well be used in practice.

5. Conclusions

A new printer calibration method is presented that is based on shell-wise subdivision of the printer gamut. The accuracy of the printed colors (mean error $\overline{\Delta E_{ab}} \approx 2.0$) is comparable with known methods if a comparable number of calibration colors is used. The mean visual errors are in the magnitude of the perceptibility threshold of $\Delta E_{ab} = 2.15$, according to Stokes et al.[9,10]

A great advantage of the new method is that once the transformation functions are established, the actual transformation of a given color is straight-forward from CIELAB to CMY; no search or inversion algorithms must be applied. Moreover, a comparatively low number of parameters of approx. 670 is sufficient to fully represent the computed transformation.

A disadvantage is that the test chart used for characterization here is organized different from traditional test charts because it must comply with the organization of the nested shells.

6. References

1. P. G. Herzog and B. Hill, "A new approach to the representation of color gamuts," in *Proc. 3rd Color Imag. Conf.*, pp. 78–81, 1995.
2. P. G. Herzog, "Analytical color gamut representations," *J. Imag. Sci. and Techn.* **40**(6):516–521, 1996.
3. H. E. Neugebauer, "Die theoretischen Grundlagen des Mehrfarbenbuchdrucks," *Z. wiss. Photogr. Photophys. Photochem.* **36**(4):73–89, 1937.
4. Y. Arai, Y. Nakano, T. Iga, and S. Usui, "A method of transformation from CIE L*a*b* to CMY value by a three-layered neural network," in *Proc. 1st Color Imag. Conf.*, pp. 41–44, 1993.
5. H. R. Kang and P. G. Anderson, "Neural network applications to the color scanner and printer calibrations," *J. Electronic Imaging* **1**(2):125–135, 1992.
6. P. G. Herzog and M. Müller, "Gamut mapping using an analytical color gamut representation," *SPIE Proceedings* **3018**, pp. 117–128, 1997.
7. M. D. Fairchild and R. S. Berns, "Image color-appearance specification through extension of CIELAB," *Color Res. Appl.* **18**:178–190, 1993.
8. M. D. Fairchild, "Visual evaluation and evolution of the RLAB color space," in *Proc. 2nd Color Imag. Conf.*, pp. 9–13, 1994.
9. M. Stokes, M. D. Fairchild, and R. S. Berns, "Precision requirements for digital color reproduction," *ACM Trans. Graphics* **11**(4):406–422, 1992.
10. M. Stokes, M. D. Fairchild, and R. S. Berns, "Colorimetrically quantified visual tolerances for pictorial images," in *TAGA Proceedings*, vol. **2**, pp. 757–777, 1992.